PHYSICAL REVIEW A **92**, 051402(R) (2015)

Rydberg blockade effects at $n \sim 300$ in strontium

X. Zhang,[1] F. B. Dunning,[1] S. Yoshida,[2] and J. Burgdörfer[2]
[1]*Department of Physics and Astronomy and the Rice Quantum Institute, Rice University, Houston, Texas 77005-1892, USA*
[2]*Institute for Theoretical Physics, Vienna University of Technology, A-1040 Vienna, Austria, European Union*
(Received 5 August 2015; published 23 November 2015)

Rydberg blockade at $n \sim 300$, is examined using strontium $n\ ^1F_3$ Rydberg atoms excited in an atomic beam in a small volume defined by two tightly focused crossed laser beams. The observation of blockade for such states is challenging due to their extreme sensitivity to stray fields and the many magnetic sublevels associated with F states which results in a high local density of states. Nonetheless, with a careful choice of laser polarization to selectively excite only a limited number of these sublevels, sizable blockade effects are observed on an $\sim$0.1 mm length scale extending blockade measurements into the near-macroscopic regime and enabling study of the dynamics of strongly coupled many-body high-n Rydberg systems under carefully controlled conditions.

DOI: 10.1103/PhysRevA.92.051402 PACS number(s): 32.80.Ee, 32.80.Rm, 34.20.Cf

The strong interactions between Rydberg atoms can lead to the formation of strongly correlated many-body systems [1,2] and have enabled the generation of entanglement between neighboring atoms [3–5], the realization of quantum gates [6,7], and the observation of many-body Rabi oscillations [8]. Detailed study of Rydberg atom–Rydberg atom interactions requires the production of Rydberg atoms with well-defined initial separations and control of their interactions by manipulating their states [9] or their separations [10]. $n \sim$ 300–500 atoms provide new opportunities to form unusually strongly interacting Rydberg systems far from the ground state and to study their time-dependent collective electron wave-packet dynamics.

Key to the production of single Rydberg atoms in well-defined regions in space is the dipole blockade [11–21] which prevents resonant excitation of nearby atoms due to the level shift afforded by the Rydberg atom already formed. This results in the formation of "superatoms" by entangling those atoms within the blockade radius. Since the strength of Rydberg-Rydberg interactions scales strongly with n [22–26], for example, the coefficient of the van der Waals (vdW) interaction, c_6/R^6, scales as $c_6 \approx n^{11}$, blockade radii also increase rapidly with n. Previous studies of the Rydberg blockade typically involved atoms with quantum numbers $n \sim 40 - 100$ resulting in blockade radii $\lesssim$10 μm [14,27]. Here we extend Rydberg blockade measurements to much larger values of n and into the macroscopic regime. Order of magnitude estimates suggest that for $n \simeq 300$ blockade radii should be $\gtrsim$0.1 mm. In this Rapid Communication we present experimental evidence for, and scaled quantum simulations of, strong blockade at such length (and energy) scales. This promises to enable the quantum entanglement of near macroscopic atomic states. The long time scales characteristic of high n states ($\sim$4 ns at $n = 300$) permits time-resolved measurements of the electron motion [9,28] that could lead to a deeper understanding of the dynamics of Rydberg-Rydberg interactions and quantum to classical crossover in Rydberg pair interactions.

The principal challenge in preparing and manipulating high-n atoms is to achieve precise control of stray and applied fields at the level of $\sim 10\ \mu\mathrm{V\,cm^{-1}}$. This we have accomplished in an apparatus that utilizes a low-density, $\sim 10^9\ \mathrm{cm^{-3}}$ strontium atom beam [29] rather than a trapped cold atomic gas. In the current work, strongly focused laser beams create an excitation volume whose size, $\sim 50 \times 50 \times 70\ \mu$m, is comparable to the blockade radius. Given the present typical beam velocities, $\sim$4–5 $\times\ 10^2\ \mathrm{ms^{-1}}$, any Rydberg atom created moves quickly out of the excitation volume requiring that, if blockade effects are to be observed, experiments be completed on time scales of $\lesssim$100 ns. High single-atom photoexcitation rates are therefore required which, as demonstrated here, can be realized when creating $n\ ^1F_3$ states. The nF states have a small quantum defect, $\sim$0.089 [26], and vdW interactions are relatively strong due to the small energy separation between an nF state and its neighboring nG state. However, nF states have $2L + 1 = 7$ magnetic sublevels and a pair of such atoms has 49 possible sublevels whose degeneracy is removed by the vdW interaction leading to energy shifts both to the blue and the red. In this regime, all sublevels of an atom pair are strongly coupled and the oscillator strength is distributed between many eigenstates with a wide range of energies, suppressing the probability for excitation of multiple atoms. Quantum calculations suggest that with a proper combination of laser polarizations such blockade effects can be pronounced.

The present apparatus (Fig. 1) is a modified version of that used in earlier experiments in this laboratory [28–30]. Strontium atoms in a tightly collimated beam are excited to selected high-n F states at the center of an interaction region defined by three pairs of copper electrodes. The three-photon excitation scheme employed, shown as an inset, utilizes the $5s5p\ ^1P_1$ and $5s5d\ ^1D_2$ intermediate states and radiation at 461, 767, and 893 nm [31]. This radiation is provided by diode laser systems whose output wavelengths are stabilized using Fabry-Perot transfer cavities locked to a polarization-stabilized He-Ne laser. The 461 and 893 nm beams are linearly polarized along the z axis indicated, the 767 nm beam is polarized along the y axis leading to creation of nF states with $M = \pm 1$. The crossed 767 and 893 nm beams are focused to $1/e^2$ diameters of $\sim$50 and 70 μm, respectively, resulting in a strongly localized excitation volume of $\sim 1.3 \times 10^{-7}\ \mathrm{cm^3}$ that typically contains tens to hundreds of ground state atoms. The 461 nm laser is not focused. Both the 461 and 767 nm lasers are tuned on resonance.

Measurements are conducted in a pulsed mode. The output of the 461 nm laser is chopped into a series of $\sim$130-ns-long pulses with a pulse repetition frequency of $\sim$20 kHz using

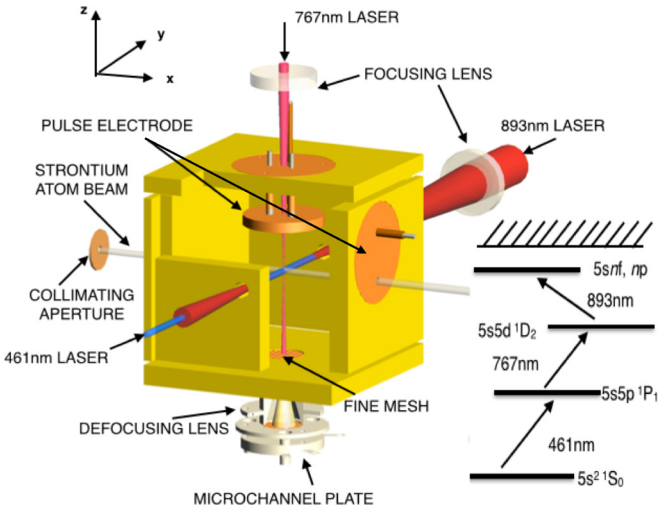

FIG. 1. (Color online) Schematic diagram of the apparatus. The inset shows the excitation scheme employed.

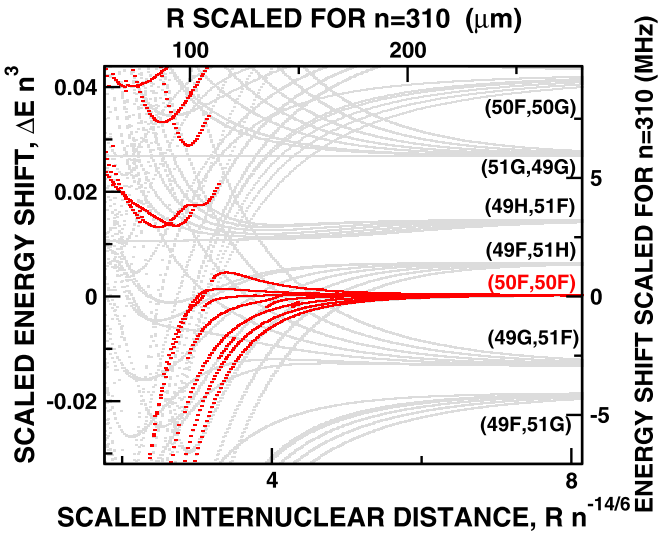

FIG. 2. (Color online) Calculated energy levels for Rydberg atom pairs with $\Lambda = M_A + M_B = 0$ near $n = 50$. The internuclear separation R is scaled by $n^{14/6}$ and the energy shift by n^{-3} (see text). Axes expressed in practical units and scaled to $n = 310$ are included for comparison to experiment. The states in red indicate those having the largest overlap with the unperturbed $50F$-$50F$ pair when expanded in the atomic basis.

an acousto-optic modulator. The other laser beams remain on at all times. Following excitation, the number of Rydberg atoms created is determined by selective field ionization by generating a slowly increasing (rise time ~ 3 μs) electric field in the excitation volume. Product electrons exit the interaction region through a series of two fine $\sim 80\%$-transparent grids and then enter a cylindrical lens that defocuses them before passing through a further grid to be detected using a microchannel plate (MCP) . Data are accumulated following many laser pulses to build up the electron number distribution. The probability that zero electrons are detected is determined by summing the number of events in which one, or more, electrons are detected and subtracting this sum from the total number of laser pulses used to acquire the data. The overall electron detection efficiency, η, could not be directly determined but was inferred from the known grid transparencies and published MCP detection efficiencies [31]. With the MCP operating with sufficient gain to saturate the count rate, the detection efficiency is estimated to be $\eta \simeq 0.51$.

The energy shift due to Rydberg atom interactions is calculated within the Born-Oppenheimer approximation. Each strontium atom is represented by a two-active-electron (TAE) Hamiltonian H_α ($\alpha = A, B$) [29]. At large internuclear distance, R, the interaction between two atoms can be approximated to leading order by the dipole-dipole interaction with $\vec{D}_\alpha$ as the total dipole moment of the atom α. Accordingly, the Hamiltonian operator of the Rydberg pair is given by

$$H = H_A + H_B + \frac{\vec{D}_A \cdot \vec{D}_B}{R^3} - 3\frac{(\vec{D}_A \cdot \hat{R})(\vec{D}_B \cdot \hat{R})}{R^3} \quad (1)$$

(atomic units used throughout, unless otherwise noted.) We checked that contributions from higher-order multipoles are negligible for the present data. Eigenenergies of Eq. (1) are calculated by numerically diagonalizing the Hamiltonian in a truncated basis expansion generated from products of atomic TAE states $|n_\alpha, L_\alpha, M_\alpha\rangle$ with $L_\alpha \leqslant 5$ and $|M_\alpha| \leqslant L_\alpha$. In the current study, both the Rydberg-Rydberg interaction and the oscillator strength from an intermediate $5s5d$ state have to be accurately evaluated. Since the electron-electron interaction plays an important role in determining the oscillator strength, the calculations need to be performed at the the TAE level. However, since computing the TAE wave functions for $n \simeq 300$ requires a great amount of computer time and memory, the numerical simulations are performed, instead, for $n \simeq 50$ and extrapolated to $n \simeq 300$ using the Coulomb scaling [30]. For the Rydberg-Rydberg interaction, similarly, we apply the Coulomb scaling to the TAE calculations for $n \simeq 50$ to compare to the (high-n) experimental data. Specifically, since characteristic energy spacings in Rydberg atoms scale as $\Delta E \sim n^{-3}$, the vdW interaction $V_{\rm vdW} \propto n^{11}/R^6$ is transformed to $V_{\rm vdW} \propto n^{-3}\tilde{V}_{\rm vdW}$ by rescaling $R = n^{14/6}\tilde{R}$ with $\tilde{V}_{\rm vdW} = \tilde{R}^{-6}$. The validity of this scaling was confirmed by independently checking directly the Rydberg-Rydberg interactions for $n \simeq 300$ using a single-active electron (SAE) model. Note that the accuracy of scaling is improved when the scaling is undertaken using the effective quantum number $n^* = n - \delta$ rather than n [26]. (For F states the difference is quite small.) Unlike for Rydberg-Rydberg interactions, the SAE model is not sufficient to accurately calculate the dipole transition from the low-lying $5s5d$ state to the Rydberg manifold requiring the use of the TAE model instead. While the scaling assumes that the potential is a homogeneous function in R, the contributions from higher-order multipoles introduce terms with different powers of R in the potential and each term has to be scaled differently. The SAE calculations, however, also reveal that interactions involving higher-order multipoles are quite small for $n = 50$ and become even less important with increasing n. Therefore, the energy diagram for $n \simeq 300$ is best approximated by scaling that obtained for $n = 50$ when neglecting all but the dipole-dipole interaction. Figure 2 shows the scaled energy shift $n^3\Delta E$ for a pair of $50F$ atoms with the internuclear axis, $\hat{R}$, aligned with the z axis and total

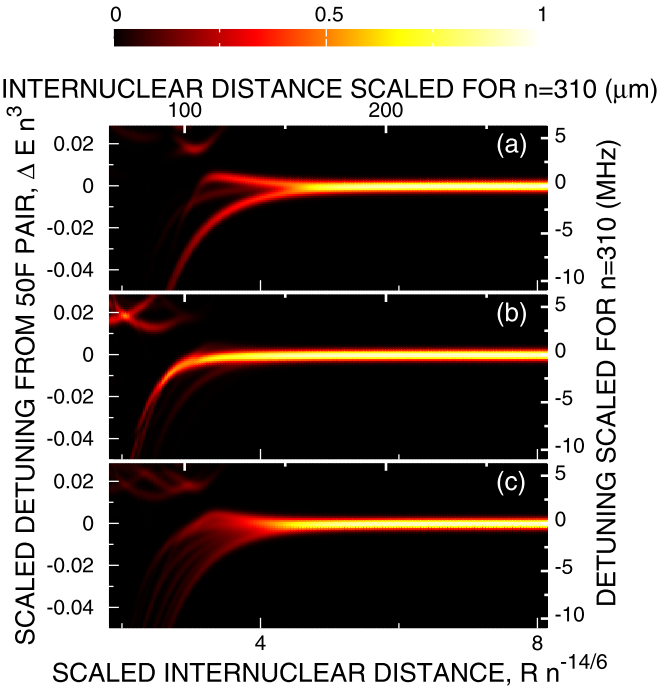

FIG. 3. (Color online) Calculated relative excitation spectra for creation of two Rydberg atoms as a function of internuclear separation R. R is scaled by $n^{14/6}$ and the detuning by n^{-3}. The laser linewidth is set to $0.002n^{-3}$ ($\sim$0.5 MHz for $n = 310$) and the spectra are normalized to 1 in the limit $R \to \infty$ with zero detuning. The atoms are assumed to be aligned (a) along the z axis and (b) along the x axis. The angular dependence is integrated in (c) (see text).

molecular magnetic quantum number, $\Lambda = M_A + M_B = 0$, as a function of the scaled distance $\tilde{R}$. Axes scaled to $n = 310$ and expressed in natural units are also included for comparison to experimental data. The vdW interaction yields both red- and blueshifted states for separations $R > 3.5n^{14/6}$, i.e., $\sim$0.12 mm for $n = 310$. For smaller values of R the intrashell coupling with nG pairs dominates and all eigenenergies are redshifted.

The oscillator strengths for excitation of the different eigenstates are laser-polarization dependent as these polarizations determine which pairs of M_α levels of the individual atoms are excited. For the present experimental configuration, the intermediate atomic $5s5d$ state is the superposition $|5D, M_\alpha = 1\rangle + |5D, M_\alpha = -1\rangle$, and the final product Rydberg state is $|nF, M_\alpha = 1\rangle + |nF, M_\alpha = -1\rangle$. Figure 3(a) shows the relative excitation strength for creation of Rydberg atoms from a $5D$-nF pair convoluted with a Gaussian profile of width $0.002n^{-3}$ ($\sim$0.5 MHz for $n = 310$). This linewidth, more than ten times smaller than the experimental value, is chosen in order to resolve small energy shifts. The product Rydberg atom pair can have quantum numbers Λ for the projection of the total angular momentum onto the internuclear axis of $0, \pm 2$ corresponding to molecular Σ or Δ states. The excitation strength summed over all substates [Fig. 3(a)] is normalized in the limit $R \to \infty$ to the blockade-free probability of single atom excitation, P_R. For values of $R < R_B = 3n^{14/6}$ ($\sim$0.1 mm for $n = 310$) the excitation strength is dramatically reduced indicating the onset of the dipole blockade. For an atom pair aligned along the x axis [Fig. 3(b)] excitation of the eigenstate with the smallest vdW shift dominates and the effective blockade radius is reduced. [Results for atom pairs aligned along the y axis are similar to those in Fig. 3(a).] Figure 3(c) presents the excitation spectrum integrated over all orientations of $\hat{R}$ assuming an isotropic distribution of atomic pairs. Below the blockade radius R_B the excitation strength is distributed over many energy-shifted eigenstates. As R decreases the excitation strength integrated over the experimental laser linewidth also decreases falling by $\sim$70% at $R = R_B = 0.1$ mm and by over 90% at $R = 70$ μm suggesting that, given the size of the present excitation volume ($\sim 50 \times 50 \times 70$ μm), sizable blockade effects should be observed.

The mean number of Rydberg atoms, $\langle N_R \rangle$, excited as a function of the 893 nm IR laser power for $n = 310$ and several different oven operating temperatures, i.e., beam densities, is shown in Fig. 4(a) and clearly deviates from the linear scaling expected in the absence of Rydberg blockade effects. At the lowest beam density where $\langle N_R \rangle$ is small, $\langle N_R \rangle < 0.15$, and hence blockade effects minimal, the number of Rydberg atoms created is directly proportional to the IR laser power. At the higher beam densities marked departures from linearity are observed as $\langle N_R \rangle$ approaches $\sim$0.5. The onset of the blockade can be quantified by the Mandel Q parameter [Fig. 4(b)]

$$Q = \frac{\langle N_R^2 \rangle - \langle N_R \rangle^2}{\langle N_R \rangle} - 1. \tag{2}$$

For uncorrelated excitation with small excitation probability, i.e., $\langle N_R \rangle / N \ll 1$, where N is the number of atoms in the excitation volume, N_R should follow a Poisson distribution and Q should be near zero. With the onset of correlations in the excitation processes, i.e., of blockade effects, Q decreases tending to -1 [32] in the limit of complete blockade, which corresponds to the creation of one and only one Rydberg atom within the blockade radius, i.e., $N_R = \langle N_R \rangle$, for each laser shot.

The dependence of Q on laser power can be simulated by a Monte Carlo approach employing the calculated angular-dependent excitation strength (Fig. 3). Since the interaction time is limited to $\sim$130 ns and much shorter than the Rabi period (>2.5 μs) for the $5s5d$ to $5snf$ transition, excitation probabilities are estimated based on Fermi's golden rule rather than by solving the optical Bloch equation. Indeed, the measured $\langle N_R \rangle$ as a function of pulse duration (not shown) shows a linear increase at low density. Considering the motion of atoms (i.e., each entering the excitation volume at different times and with slowly varying internuclear distances), the excitation dynamics is considered to be incoherent. This is indicated in the inset of Fig. 4(a). The mean Rydberg number $\langle N_R \rangle$ at a given laser intensity is proportional to density implying no sign of collective (cooperative) excitation. In the simulations, the probability P for exciting N_R Rydberg atoms from N atoms randomly placed within the interaction volume, V_{ex}, is calculated. The motion of atoms is not considered and the atom distribution in the excitation volume is assumed to be uniform. The excitation of multiple atoms is assumed to be sequential since the probability for the simultaneous excitation of multiple atoms is very small in the current setup. In practice, the probability P depends on the state of the N particle ensemble at the site of excitation.

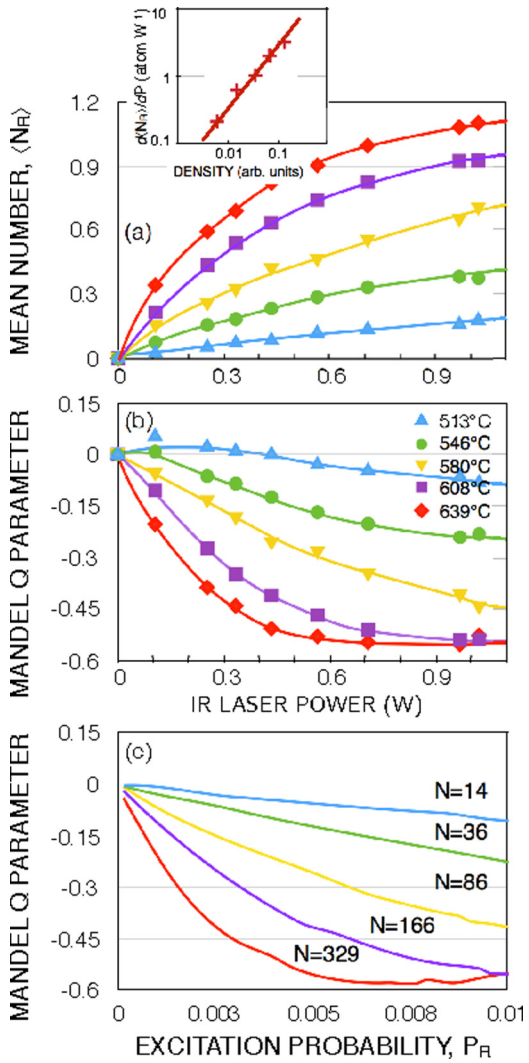

FIG. 4. (Color online) (a) Mean number, $\langle N_R \rangle$, of $n \sim 310$ Rydberg atoms excited by a 130-ns-long 461 nm laser pulse as a function of 893 nm IR laser power for the oven operating temperatures indicated. The inset shows the mean Rydberg atom number created per unit laser power $\mathcal{P}$, $d\langle N_R \rangle / d\mathcal{P}$ ($\mathcal{P} = 0$), for small laser powers as a function of beam density showing a linear increase with density. (b) Measured Q values. The results in (a) and (b) are corrected for the detection efficiency η. (c) Calculated Q values versus Rydberg excitation probability. The calculations assume the blockade probability $1 - P_2$ is reduced by 20% from the theoretical value (see text). N specifies the assumed number of ground state atoms present in the excitation volume.

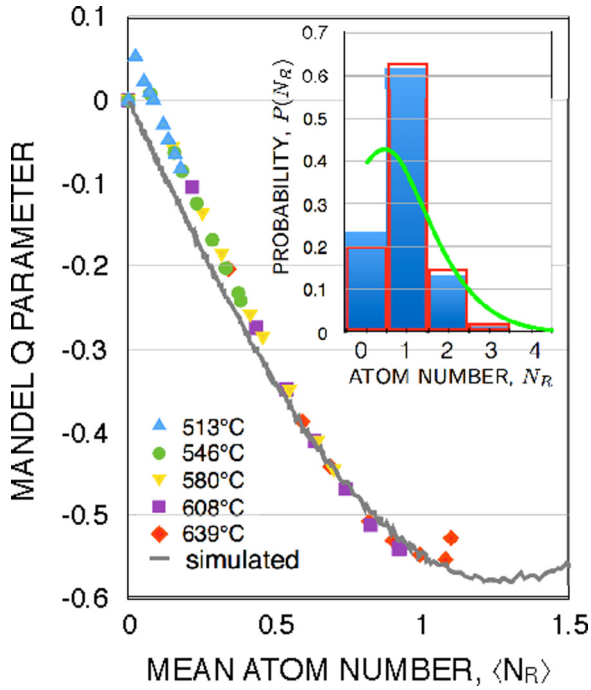

FIG. 5. (Color online) Measured Q values expressed as a function of $\langle N_R \rangle$. The solid line shows the calculated values. The inset presents a typical Rydberg number distribution for $\langle N_R \rangle \sim 1$ (filled histogram: $P = 0.9W$, $T = 639\,^{\circ}\mathrm{C}$) together with a calculated distribution (open histogram: $N = 329$, $P_R = 0.005$, for the same $\langle N_R \rangle$). The line shows a Poissonian distribution for $\langle N_R \rangle = 1$.

If no prior excitation has occurred, $P = P_R$ and $N_R = P_R N$ where P_R is the single-Rydberg-atom excitation probability. If one or more atoms in the ensemble are already excited, the excitation probability becomes $P = P_R P_2$ where P_2 is determined by the normalized angle- and distance-dependent pair excitation strength (similar to Fig. 3) using the overall transform-limited effective experimental laser linewidth of ~ 8 MHz. For $N_R > 2$, the excitation probability of N_R atoms depends on the sequence in which the N_R atoms are created. Therefore, this sequence as well as the combination of N_R atoms has to be randomized. The Rydberg number distribution is obtained by considering a large number of realizations of the excitation sequence. As in the experiment [Fig. 4(b)], the calculated Mandel Q parameter [Fig. 4(c)] decreases with increasing density and with P_R, i.e., laser power. The number, N, of atoms in the excitation volume used in the simulation was derived from the vapor pressure corresponding to the oven temperatures indicated in Fig. 4(b). To obtain the best agreement with the measured Q values the blockade probability, $P_B = 1 - P_2$, was reduced by 20% from the calculated value. Since the measured Q parameter scales linearly with the effective detection efficiency η, a 20% error in η could account for the corresponding reduction in P_B. Other factors that might contribute to the discrepancies include inhomogeneities in laser intensity over the excitation volume and residual stray fields.

The Mandel Q parameter should be governed by $\langle N_R \rangle$, i.e., Q should be identical for different combinations of target density and laser intensity that give rise to the same value of $\langle N_R \rangle$. While, as shown in Fig. 5, this is indeed the case, the Q value does not approach -1 as $\langle N_R \rangle \to 1$ even at high oven temperatures but rather reaches the limiting value $Q \sim -0.55$ indicating blockade is not complete. This is further demonstrated in the inset in Fig. 5 which shows a Rydberg number distribution typical of those measured for $\langle N_R \rangle \sim 1$ together with a theoretical prediction and a Poisson distribution with $\langle N_R \rangle = 1$. Whereas a majority of laser pulses lead to the creation of a single Rydberg atom, there remains a small probability for creation of zero or multiple Rydberg atoms. Nonetheless, the probability for exciting a single Rydberg atom in the excitation volume is sizable $P(N_R = 1) \simeq 0.62$. When using

two well-separated Rydberg excitation volumes, the probability of producing a single atom in each remains relatively large [$P(N_R = 1)^2 \simeq 0.38$]. Increases in detection efficiency through apparatus redesign to reduce the number and opacity of the grids through which the electrons pass en route to the MCP should allow good discrimination against events in which fewer than, or more than, two Rydberg atoms are created. The conditional probability that, if two Rydberg atoms are detected, they are created in separate regions, $P(N_R = 1)^2/[P(N_R = 1)^2 + 2P(N_R = 0)P(N_R = 2)]$, will approach $\simeq 0.86$. Thus, even though the blockade is not complete, it is sufficient to allow the efficient creation (and identification) of Rydberg atom pairs with well-defined initial separations. Having created such pairs, their interactions can be dramatically increased by simultaneously exciting both to states of much higher n using a carefully tailored sequence of short electric field pulses [9], enabling detailed studies of the dynamics of the resulting strongly interacting and strongly correlated atom pairs.

Summarizing, we have found compelling evidence of the Rydberg blockade in very high Rydberg states in strontium. The blockade radius, ~ 0.1 mm, is of almost macroscopic scale. Results for the number distribution and Mandel Q parameter are in good accord with scaled quantum simulations performed for lower $n = 50$. A similar localization approach might be applied in a cold strontium atom cloud where the atomic densities can be much higher and the atomic motions are much slower. However, the optical access required for laser cooling and trapping will require careful electrode design to achieve the level of field control necessary to create and manipulate very high-n Rydberg atoms.

This research is supported by the NSF under Grant No. 1301773, by the Robert A. Welch Foundation under Grant No. C-0734, by the FWF (Austria) under Grant No. P23359-N16, and by SFB-049 NextLite. The Vienna cluster was used for the calculations.

[1] T. M. Weber, M. Honing, T. Niederprum, T. Manthey, O. Thomas, V. Guarrera, M. Fleischhauer, G. Barontini, and H. Ott, Nat. Phys. **11**, 157 (2015).
[2] A. Urvoy, F. Ripka, I. Lesanovsky, D. Booth, J. P. Shaffer, T. Pfau, and R. Löw, Phys. Rev. Lett. **114**, 203002 (2015).
[3] D. Møller, L. B. Madsen, and K. Mølmer, Phys. Rev. Lett. **100**, 170504 (2008).
[4] T. Wilk, A. Gaëtan, C. Evellin, J. Wolters, Y. Miroshnychenko, P. Grangier, and A. Browaeys, Phys. Rev. Lett. **104**, 010502 (2010).
[5] X. L. Zhang, L. Isenhower, A. T. Gill, T. G. Walker, and M. Saffman, Phys. Rev. A **82**, 030306 (2010).
[6] M. Müller, I. Lesanovsky, H. Weimer, H. P. Büchler, and P. Zoller, Phys. Rev. Lett. **102**, 170502 (2009).
[7] L. Isenhower, E. Urban, X. L. Zhang, A. T. Gill, T. Henage, T. A. Johnson, T. G. Walker, and M. Saffman, Phys. Rev. Lett. **104**, 010503 (2010).
[8] Y. O. Dudin, L. Li, F. Bariani, and A. Kuzmich, Nat. Phys. **8**, 790 (2012).
[9] F. B. Dunning, J. J. Mestayer, C. O. Reinhold, S. Yoshida, and J. Burgdörfer, J. Phys. B **42**, 022001 (2009).
[10] Y.-Y. Jau, A. M. Hankin, T. Keating, I. H. Deutsch, and G. W. Biedermann, arXiv:1501.03862.
[11] D. Jaksch, J. I. Cirac, P. Zoller, S. L. Rolston, R. Côté, and M. D. Lukin, Phys. Rev. Lett. **85**, 2208 (2000).
[12] T. F. Gallagher and P. Pillet, in *Advances in Atomic, Molecular and Optical Physics*, edited by E. Arimondo *et al.* (Academic, New York, 2008), Vol. 56, pp. 161–218.
[13] D. Comparat and P. Pillet, J. Opt. Soc. Am. B **27**, A208 (2010).
[14] M. Saffman, T. G. Walker, and K. Mølmer, Rev. Mod. Phys. **82**, 2313 (2010).
[15] D. Tong, S. M. Farooqi, J. Stanojevic, S. Krishnan, Y. P. Zhang, R. Côté, E. E. Eyler, and P. L. Gould, Phys. Rev. Lett. **93**, 063001 (2004).
[16] E. Urban, T. A. Johnson, T. Henage, L. Isenhower, D. D. Yavuz, T. G. Walker, and M. Saffman, Nat. Phys. **5**, 110 (2009).
[17] M. Robert-de-Saint-Vincent, C. S. Hofmann, H. Schempp, G. Günter, S. Whitlock, and M. Weidemüller, Phys. Rev. Lett. **110**, 045004 (2013).
[18] A. M. Hankin, Y.-Y. Jau, L. P. Parazzoli, C. W. Chou, D. J. Armstrong, A. J. Landahl, and G. W. Biedermann, Phys. Rev. A **89**, 033416 (2014).
[19] N. Malossi, M. M. Valado, S. Scotto, O. Morsch, E. Arimondo, and D. Ciampini, J. Phys. Conf. Ser. **497**, 012031 (2014).
[20] D. Barredo, S. Ravets, H. Labuhn, L. Béguin, A. Vernier, F. Nogrette, T. Lahaye, and A. Browaeys, Phys. Rev. Lett. **112**, 183002 (2014).
[21] H. Labuhn, S. Ravets, D. Barredo, L. Béguin, F. Nogrette, T. Lahaye, and A. Browaeys, Phys. Rev. A **90**, 023415 (2014).
[22] A. Reinhard, T. C. Liebisch, B. Knuffman, and G. Raithel, Phys. Rev. A **75**, 032712 (2007).
[23] J. Stanojevic, R. Côté, D. Tong, E. E. Eyler, and P. L. Gould, Phys. Rev. A **78**, 052709 (2008).
[24] K. Singer, J. Stanojevic, M. Weidemüller, and R. Côté, J. Phys. B **38**, S295 (2005).
[25] R. Côté, A. Russell, E. E. Eyler, and P. L. Gould, New J. Phys. **8**, 156 (2006).
[26] C. L. Vaillant, M. P. A. Jones, and R. M. Potvliege, J. Phys. B **45**, 135004 (2012).
[27] C. Tresp, P. Bienias, S. Weber, H. Gorniaczyk, I. Mirgorodskiy, H. P. Büchler, and S. Hofferberth, Phys. Rev. Lett. **115**, 083602 (2015).
[28] M. Hiller, S. Yoshida, J. Burgdörfer, S. Ye, X. Zhang, and F. B. Dunning, Phys. Rev. A **89**, 023426 (2014).
[29] S. Ye, X. Zhang, F. B. Dunning, S. Yoshida, M. Hiller, and J. Burgdörfer, Phys. Rev. A **90**, 013401 (2014).
[30] S. Ye, X. Zhang, T. C. Killian, F. B. Dunning, M. Hiller, S. Yoshida, S. Nagele, and J. Burgdörfer, Phys. Rev. A **88**, 043430 (2013).
[31] A. Müller, N. Djuric, G. H. Dunn, and D. S. Belic, Rev. Sci. Instrum. **57**, 349 (1986).
[32] L. Mandel, Phys. Rev. Lett. **49**, 136 (1982).